

DANISH METEOROLOGICAL INSTITUTE

SCIENTIFIC REPORT

99-3

European Stratospheric Monitoring Stations in the Arctic II

CEC Environment and Climate Programme

Contract ENV4-CT95-0136

DMI contributions to the project

**Niels Larsen
Bjørn M. Knudsen
Paul Eriksen
Ib Steen Mikkelsen
Signe Bech Andersen
Torben Stockflet Jørgensen**



COPENHAGEN 1999

Danish Meteorological Institute, Division of Middle Atmosphere Research,
Lyngbyvej 100, DK-2100 Copenhagen Ø, Denmark

ISBN 87-7478-390-4
ISSN 0905-3263
ISSN 1399-1949 (ONLINE)

European Stratospheric Monitoring Stations in the Arctic II ESMOS /Arctic II

CEC Environment and Climate Programme Contract ENV4-CT95-0136
Contributions to the project by the Danish Meteorological Institute

This CEC project has been accomplished in collaboration with

Alfred Wegener Institute, Potsdam, Germany
University of Rome "La Sapienza, Rome, Italy
University of Bremen, Germany
Norwegian Institute for Air Research, Kjeller, Norway
Institute for Atmospheric Physics, Kühlungsborn, Germany
Finnish Meteorological Institute, Sodankylä, Finland
National Physical Laboratory, Teddington, United Kingdom
Communications Research Laboratory, Tokyo, Japan
National Center for Atmospheric Research, Boulder, Co., USA
University Courses at Svalbard, Norway
University of New York at Stony Brook, NY, USA
University of Wyoming, Laramie, Wy. USA
Swedish Environmental Research Institute, Sweden
University of Thessaloniki, Greece

Project period: 1 February 1996 – 31 January 1999

Introduction and objectives

The ESMOS/Arctic II project addresses the issues of Arctic ozone depletion and its causes. Within the project changes in the composition of the Arctic stratosphere have been observed by a network of stations and analysed by performing long-term measurements, assuring instrumental quality standards, supplemented by analysing collected data sets, performing case studies, and stratospheric aerosol and chemical trajectory modelling. Collected data have been shared via European and international databases.

The growing problem of polar and mid latitude ozone depletion was reconfirmed by the recent WMO assessment reports¹. The necessity was realised to observe the Arctic stratosphere in order to study the degree and processes of the decline of stratospheric ozone, which might come abrupt, and how such decline might affect highly populated European regions in high and middle latitudes.

¹ Scientific Assessment of Ozone Depletion: 1994 and 1998, WMO reports No. 37 and 44, Geneva, 1995 and 1999

Particularly the objectives of the project have been to

- investigate chemical and dynamical processes in the lower Arctic stratosphere within the European Stratospheric Monitoring Stations (ESMOS) network, which stretches from 79°N (Spitsbergen) to 44°N (Haute Provence).
- perform modelling studies to investigate the processes controlling the ozone loss
- determine the spatio-temporal extend of chemical perturbations in the lower and lowest part of the stratosphere, where air can be transported easily to mid-latitudes.
- assess latitudinal trends in ozone and related trace species.
- establish an Arctic network of backscattersonde and aerosol lidar stations to improve our knowledge about the occurrence of Polar Stratospheric Clouds (PSC) and their formation processes.
- contribute to the observation of solar UV radiation with a high latitude station.

The ESMOS/Arctic stations at Thule (Pituffik), Greenland (hosted by DMI), Ny-Ålesund/Spitsbergen, and the ALOMAR observatory at Andenes/Norway are integral parts of the global Network for the Detection of Stratospheric Change (NDSC) and some of the most modern ground based stratospheric observation stations available. The combined DMI stratospheric observatory and the SRI lidar facility at Sondre Stromfjord (Kangerlussuaq), Greenland is an Arctic NDSC station as well as the Sodankylä observatory in Finland. ESMOS has a leading role within NDSC due to the state of the art equipment and data quality checks and assurance. This network, initiated in the beginning of the 1990's comprises a limited set of high-quality remote-sensing research stations in the tropics, at mid latitudes, and in the polar regions of both hemispheres. It employs a number of selected instruments of verified high quality, including UV/visible and infrared spectrometers for measurements of column abundance of ozone and a large number of trace gases, ozone and aerosol lidars, microwave sounders, and facilities to perform balloonborne ozone soundings. One of the key issues of the network is the assurance of high-quality standards and the determination of measurements techniques and procedures (like data evaluation algorithms) to further improve quality standards in order to produce long-term data sets of proven stable quality.

Within NDSC the objectives are to

- observe changes in the physical and chemical state of the stratosphere
- discern and understand the causes of the changes
- provide independent calibration of satellite sensors
- obtain data that can be used to test and improve stratospheric chemical and dynamical models, thereby enhancing confidence in their predictive and assessment capabilities.

The DMI stratospheric observatory at Thule Air Base, Greenland (76.5 N, 68.8 W), has been appointed as one of the arctic primary NDSC sites. The DMI possess buildings on the South Mountain and at the main base at Thule, fully equipped with communication (telephone, fax, internet) and computational facilities. The DMI has contributed to the

instrumentation of the site by a UV-visible spectrometer (SAOZ) for ozone and other trace gas measurements. The DMI also operates an UV spectroradiometer at Thule for measurements of UVB radiation, and DMI has installed instrumentation for balloonborne measurements of ozone. In collaboration with the DMI the University of Rome operates an aerosol lidar. The DMI has collaborated for several years with the University of Wyoming on balloonborne stratospheric aerosol and cloud particle measurements from the NDSC station at Thule. At Sondre Stromfjord DMI operates a Brewer instrument for measurements for column ozone, and has collaborated for many years with SRI-International (California) on aerosol lidar measurements and investigations of stratospheric winds and mountain waves employing the SRI radar facility

DMI has participated, by contracts to the EU-commission, from the start of the ESMOS-project and through its predecessors, "Experimentation related to polar stratospheric clouds", (contract STEP-CT90-0078), "Investigations of ozone, aerosols, and clouds in the Arctic stratosphere" (contract EV5V-CT92-0074; DMI scientific report 95-3), and "European Stratospheric Monitoring Stations in the Arctic" (contract EV5V-CT93-0333; DMI scientific report 96-11). Stratospheric measurements from the DMI observatories in Greenland, including Scoresbysund (Illoqqortoormiut), have been part of the major European field campaigns "European Arctic Stratospheric Experiment on Ozone (EASOE, 1991-1992), Second European Stratospheric Arctic and Mid-latitude Experiment (SESAME, 1994-1995), and Third European Stratospheric Experiment on Ozone (THESEO, 1998-1999).

Background.

Ozone in the stratosphere, the ozone layer, protects the surface of the Earth from harmful solar ultraviolet (UV) radiation. Research during the past decade has revealed that a combination of specific meteorological conditions and atmospheric chemical processes may lead to strong depletion of the ozone layer in polar regions in both hemispheres during winter and early spring². Ozone depleted air from polar regions has the potential to mix with mid-latitude air, causing a decrease in ozone concentrations at lower latitudes, e.g. over Europe. Over Antarctica the well-known ozone hole develops every austral spring with the total ozone column reduced by more than 50 % and nearly total ozone destruction between 15 and 20 km altitude. During the some of the winters in the 1990's large ozone depletions have also been observed in the Arctic, as described in this report, although not as severe and regularly as observed over Antarctica.

A key-process for strong chemical ozone destruction is the formation for polar stratospheric clouds (PSC) in combination with a relatively stable polar vortex and the presently elevated concentrations of chlorine and bromine, originating to a large extent from man-made CFC and Halon gases. On the surfaces of the cloud particles, chlorine containing compounds (mainly ClONO₂ and HCl) are converted in heterogeneous chemical reactions into reactive forms which catalytically destroy ozone in the presence of sunlight. During winter strong winds circle around the poles at altitudes above ≈ 15 km in a more or less regular pattern, forming the polar vortex. Inside the vortex the

² WMO, 1994, 1999

stratospheric air is relatively isolated from mixing with air from lower latitudes and temperatures occasionally drop sufficiently low for PSCs to form, leading to activation of chlorine compounds inside the vortex. When sunlight returns to the polar regions ozone inside the vortex is chemically depleted until the vortex breaks up later in spring and the catalytic reactions are terminated.

Compared to Antarctica the main reason that regular Arctic ozone holes have not appeared is mainly related to higher temperatures and more sporadic PSC formation in combination with a weaker polar vortex. Climate models have recently predicted that increased concentrations of greenhouse gases in the atmosphere and depletion of the ozone layer may cause lower temperatures in the stratosphere and more widespread PSC formation together with more stable and long-lasting vortex formation in the Northern Hemisphere³. Although chlorine concentrations in the atmosphere are expected to peak around the turn of the century, decreasing temperatures in a future climate may cause a substantial delay of a recovery of the ozone layer. Recent investigations have revealed that denitrification in the stratosphere, i.e. the irreversible removal of reactive nitrogen species by gravitational settling of PSC particles, have led to increased ozone destruction in the Arctic⁴. It has also been observed that during cold winters the polar vortex may travel widely over populated areas of northern Europe. Whereas denitrification is not a regularly occurring phenomenon in the present Arctic stratosphere, generally decreasing temperatures and more frequent PSC formation could likely more often lead to denitrification and thereby stronger ozone depletion in the future.

The perspective of couplings between global climate changes and ozone depletion calls for long-term monitoring of the stratosphere, which is in focus within the NDSC and ESMOS framework. The nature of the problem implies scientific research in various directions, and DMI has contributed to the ESMOS/Arctic II project by meteorological analysis (vortex position and stratospheric temperatures, mixing of air between high and lower NH latitudes, air parcel trajectory calculations), measurements of total column ozone and other trace gases, balloonborne measurements of the vertical ozone profile, microphysical modelling and observations of PSC, and measurements of UV-B radiation on the surface of the Earth. The following sections describe the results obtained in these fields.

Meteorological data analysis

Potential vorticity (PV) and pressure have been calculated in a 2.5°x2.5° latitude-longitude grid north of 30°N on the 350, 380, 400, 435, 475, 550 and 675K isentropic levels. A 1, 2, 3, 4, 5 and 8 day forecast for 350, 475, 550 and 675K has also been available in real time. These data have been calculated from 1 November to 30 April during the winters 1995/96, 1996/97, 1997/98 and 1998/99. Files with higher-resolution PV data interpolated to each measurement site are also available.

³ Shindell, D.T., D.Rind, and P. Lonergan, Increased polar stratospheric ozone losses and delayed eventual recovery owing to increasing greenhouse-gas concentrations, *Nature* 392, 589-592, 1998.

⁴ Waibel, A.E. et al., Arctic ozone loss due to denitrification, *Science* 283, 2064-2069, 1999.

An example of the location of the polar vortex (in terms of strong latitudinal gradients in PV) on the 475 K potential temperature surface is shown in Figure 1 on a map of the polar region north of 40°N from 15 February 1997 at 12.00 UT. The vortex is elongated and at the center the temperatures are sufficiently low for potential formation of PSCs (inside the thick line contour, marking the 195 K isotherm).

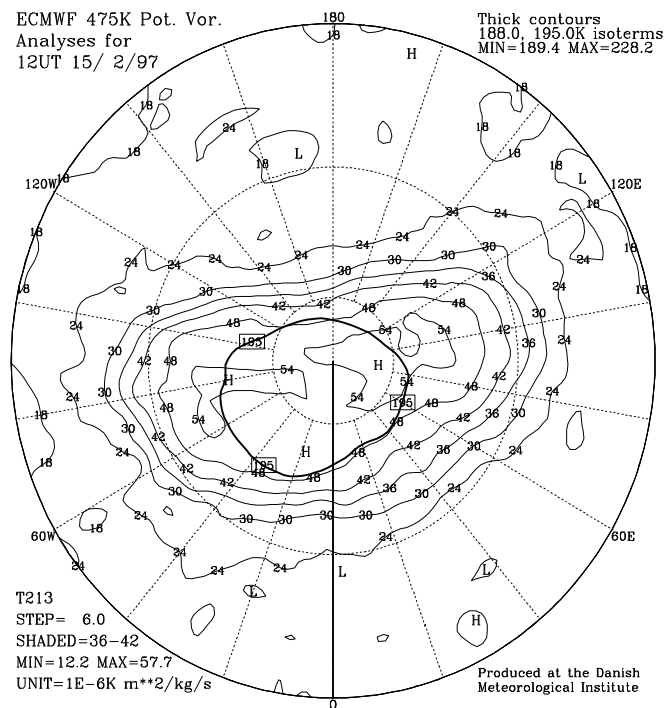


Figure 1 Contour map of potential vorticity (thin lines) and the 195 K isotherm (PSC threshold temperature, thick line). Latitude circles at 40°, 60°, and 80°N.

Figure 2 shows the temporal development of the size of the geographical area on the 475K surface where polar stratospheric clouds (PSC) could potentially form predicted from ECMWF temperatures, in the winters from 91/92 to 97/98. It is evident that there was an unusually large potential for PSC-formation during March in the winter 1996/97 and also large areas of potential PSC formation in winter 1995/96.

Ten day backward isentropic trajectories have been calculated at the 350, 380, 400, 435, 475, 550 and 675K isentropic levels with endpoints on all ESMOS measurement sites and on an equal area grid with 118 gridpoints north of 30°N. These trajectories are calculated for the same period as the other isentropic data mentioned above

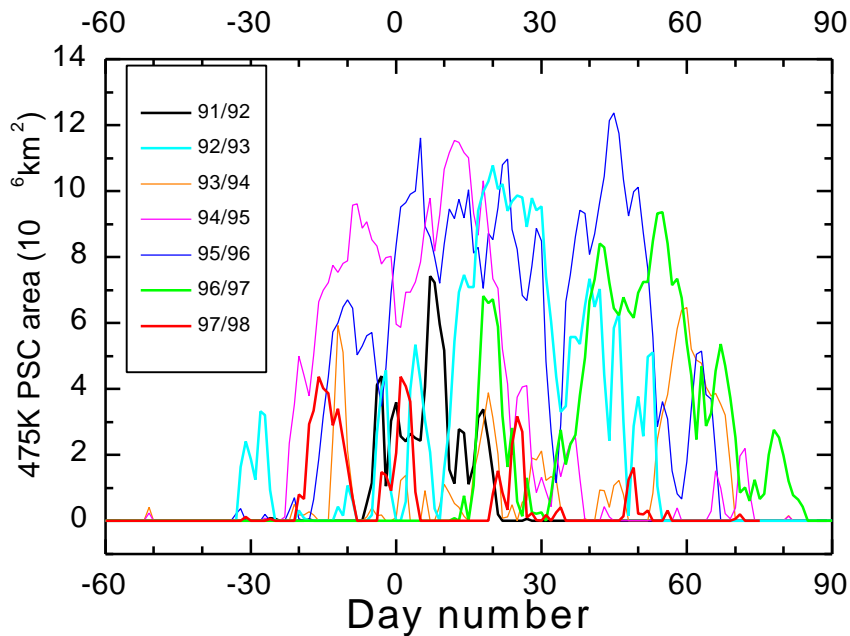


Figure 2 Size of the geographical area on the 475 K potential temperature surface, where PSC could potentially form, calculated for 7 Arctic winters.

Ozone and Trace Gas measurements and data interpretation

During the ESMOS/Arctil II project period 58 ozone sondes were launched at Thule by the DMI (supplemented by 182 launches from Scoresbysund -Illoqqortoormiut). Many of the sondes were part of the coordinated efforts within the MATCH approach

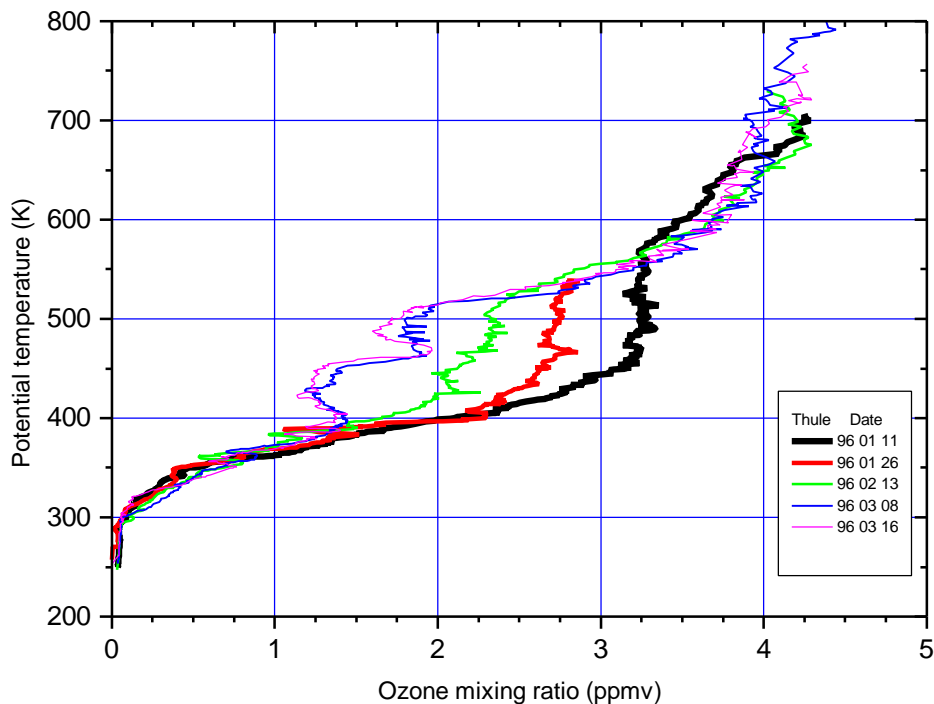


Figure 3 Examples of vertical ozone profiles from balloonborne soundings performed at Thule in winter-spring 1996 (inside the polar vortex). Large depletions of the ozone mixing ratio (up to 50 %) are observed in the altitude range 400-550 K, corresponding to 15-22 km

of the concurrent EU-project "Ozone soundings as a tool for detecting ozone change", where the same airparcels were sounded at successive stations in order to obtain Lagrangean measurements of the chemical ozone depletion.

The results from a sequence of ozone soundings at Thule, obtained during the first three months of 1996 when this station was inside the polar vortex, show the severe ozone depletion during this period, cf. Figure 3 displaying five vertical ozone mixing ratio profiles. This plot indicates that in the altitude range of 400 - 550 K potential temperature (app. 15 - 22 km) up to 50 % of the ozone concentrations were depleted. This is a conservative estimate and does not take into account the diabatic cooling inside the vortex which normally bring down airmasses with higher ozone mixing ratios and to some degree compensate for the chemical destruction.

By including ozone soundings from other ESMOS stations this picture of severe Arctic ozone depletion in the first 4 months of 1996 is confirmed. Figure 4 shows the ozone mixing ratios at potential temperature 500 K (app. 20 km altitude), measured by ozone soundings at Thule, Ny Ålesund, Scoresbysund, and Sodankylä as function of time. Measurements obtained inside the polar vortices (red symbols) again indicate the strong ozone depletions.

As for the winter 1995/96, strong ozone depletion was observed inside the Arctic polar vortex around 500 K potential temperature altitude in winter 1996/97. This is

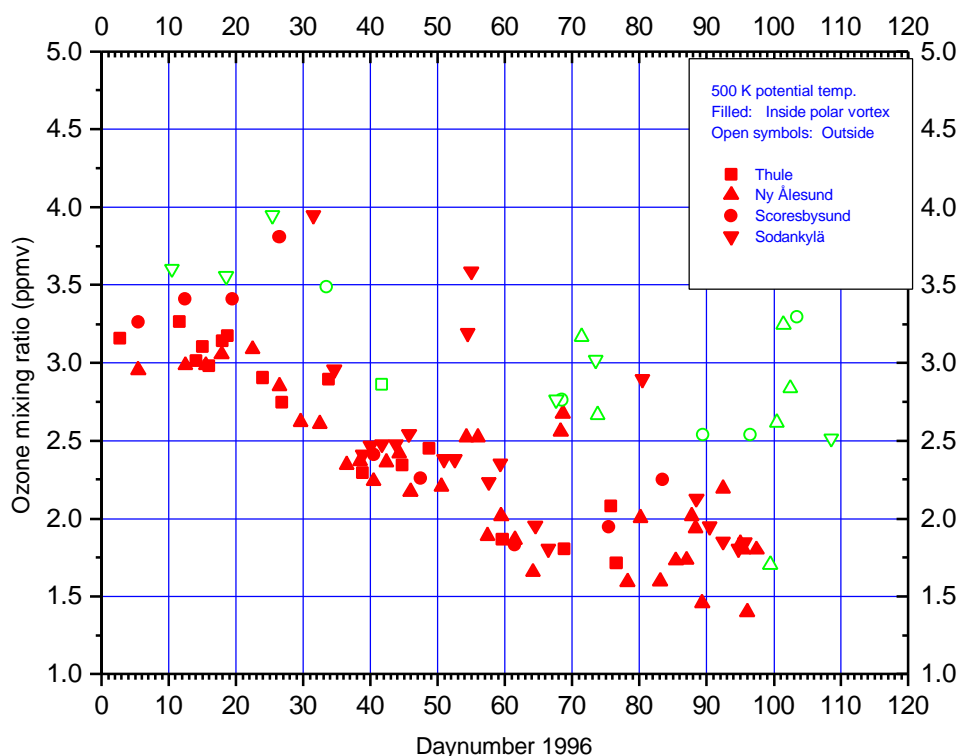


Figure 4 Ozone mixing ratios at potential temperature 500 K (app. 20 km altitude), measured by balloonborne ozone sondes at Thule, Ny Ålesund, Scoresbysund, and Sodankylä during the first 4 months of 1996. A significant decrease in ozone mixing ratio inside the polar vortex (red symbols) is observed. The chemical ozone depletion could be even larger since the measurements have not been corrected for diabatic descent which tends to compensate for chemical destruction.

clearly demonstrated in Figure 5, showing ozone mixing ratios on the 500 K potential temperature surface, obtained from ozone soundings at 5 Arctic stations inside (red symbols) and outside (green symbols) the polar vortex.

The winter 1996/97 was quite unusual with late vortex formation and polar stratospheric cloud (PSC) development and subsequent record low temperatures in March (cf. Figure 2). Ozone depletion within the Arctic vortex has been determined by DMI using data from 530 ozone soundings from all stations the Arctic vortex (Knudsen et al., 1998). These are the European stations north of 60°N including Greenland and all North Atlantic stations except Bear Island, all Canadian stations except Edmonton, and two Russian stations. The diabatic cooling was calculated with the Morcrette radiation scheme using PV-potential temperature mapped ozone mixing ratios and the large ozone depletions, especially at the center of the vortex where most PSC existence was predicted, enhanced the diabatic cooling by up to 80%.

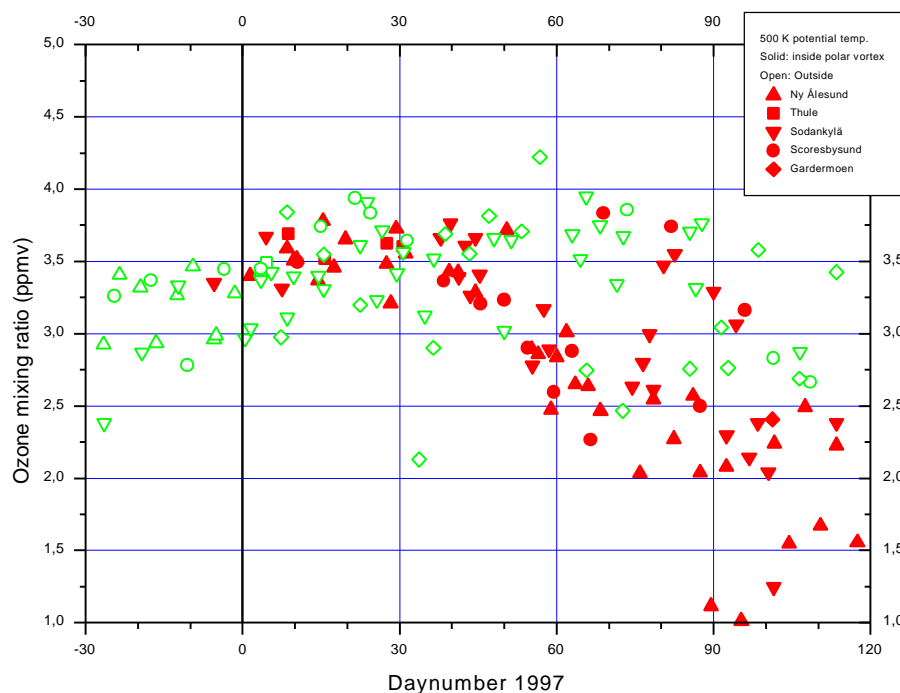


Figure 5. Ozone mixing ratios at potential temperature 500 K (app. 20 km altitude), measured by balloonborne ozone sondes at Thule, Ny Ålesund, Scoresbysund, Sodankylä, and Gardermoen during the first 4 months of 1997.

In Figure 6 the ozone mixing ratio, corrected for diabatic cooling, are shown for air masses ending at 375, 400, 425, 450, 475, 500, 525, and 550K on April 11, 1997. The average vortex chemical ozone depletion from January 6 to April 6 was 33, 46, 46, 43, 35, 33, 32 and 21 % in air masses ending at 375, 400, 425, 450, 475, 500, 525, and 550K (about 14 - 22 km). This depletion was corrected for transport of ozone

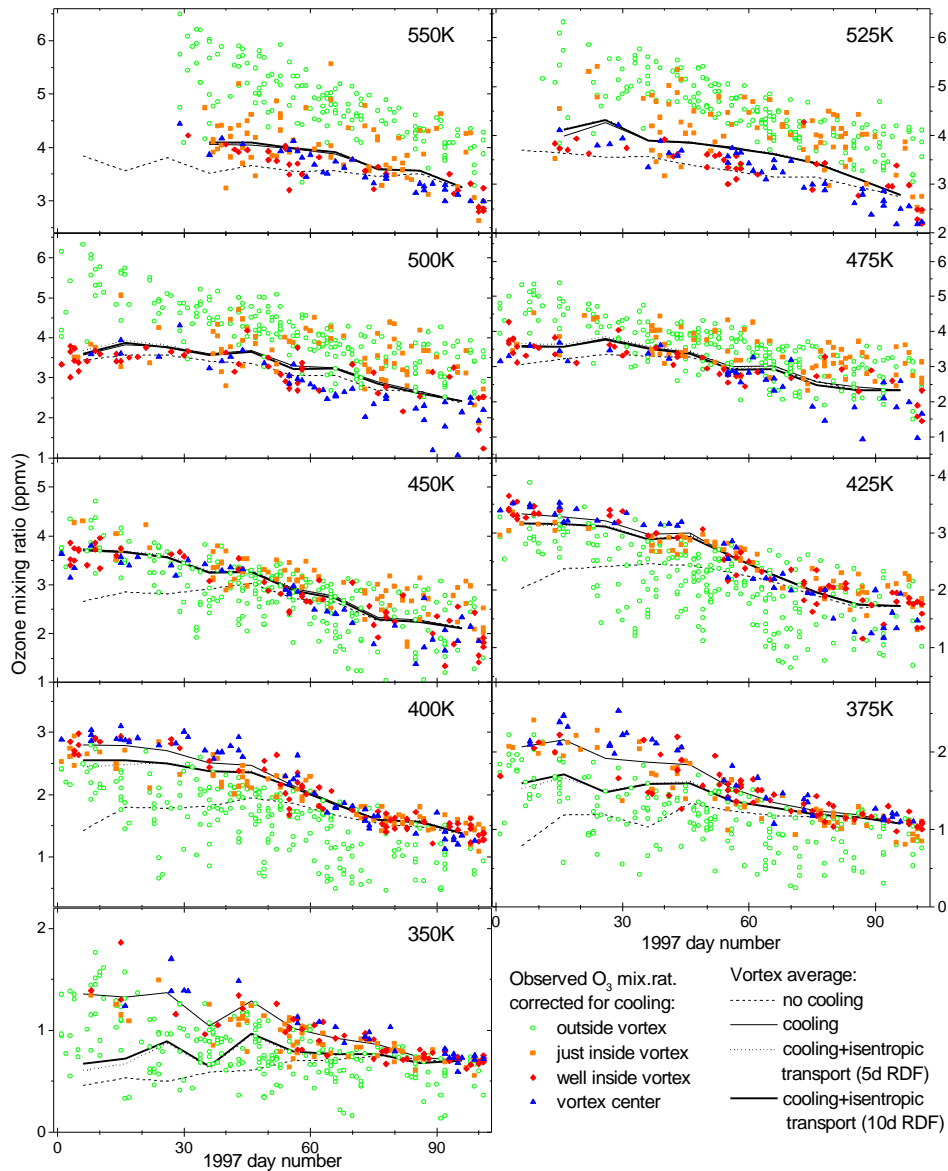


Figure 6 Observed ozone mixing ratios corrected for cooling are shown with symbols. The observations inside the vortex have been divided according to which third of the vortex area they belong. The averaged vortex mixing ratio is also shown both with (thin, solid line) and without (dashed line) correction for cooling. Corrections for quasi-isentropic transport using 5 day (dotted line) and 10 day RDF calculations (thick, solid line) have also been applied. Outside the vortex, the vortex cooling rates have been applied as well so that at any instance the mixing ratios inside and outside the vortex are on the same isentrope and can thus be compared. This creates an apparent decrease in the mixing ratios outside the vortex, which is not real, because average cooling rates outside the vortex are much smaller than inside.

across the vortex edge calculated with reverse domain-filling (RDF) trajectories. (In fact, 375K is below the vortex, but the calculation method is applicable at this level with small changes). The column integrated chemical ozone depletion was about 92 DU (21%), which is comparable to the depletions observed during the previous four winters.

A SAOZ UV-vis spectrometer has been in operation by DMI in Thule since September 1990. Figure 7 illustrates the ozone column measurements in spring 1996, compared to the TOMS version 6 satellite measurements, averaged in the period 1978-1988.

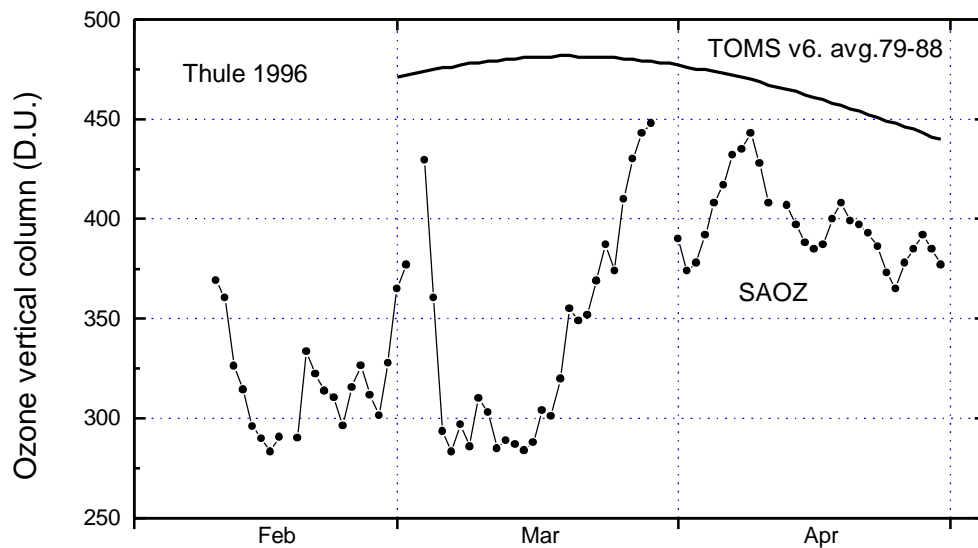


Figure 7 SAOZ ozone measurements for Feb.- Apr. 1996. shows very low ozone in the presence of the vortex in late Feb. and early Mar. For these periods also NO_2 columns were low.

Figure 8 shows the vertical columns of ozone and NO_2 measured by in spring 1997, together with ECWMF potential vorticity at 475 K indicative of the presence of the vortex over the station, the temperature of the 50 hPa level, and finally the height of the 250 hPa pressure level is shown in order to distinguish variations of the vertical columns due to variations in pressure. In February and March the polar vortex was above Thule most of the time and low ozone values are seen through out the period. Temperatures low enough for polar stratospheric clouds to form are only seen above Thule for a shorter period in February. The lowest ozone values measured in spring since the instrument was installed were seen on March 20, 1997. This however coincides with high pressure and should therefore not be regarded entirely as a sign of ozone depletion.

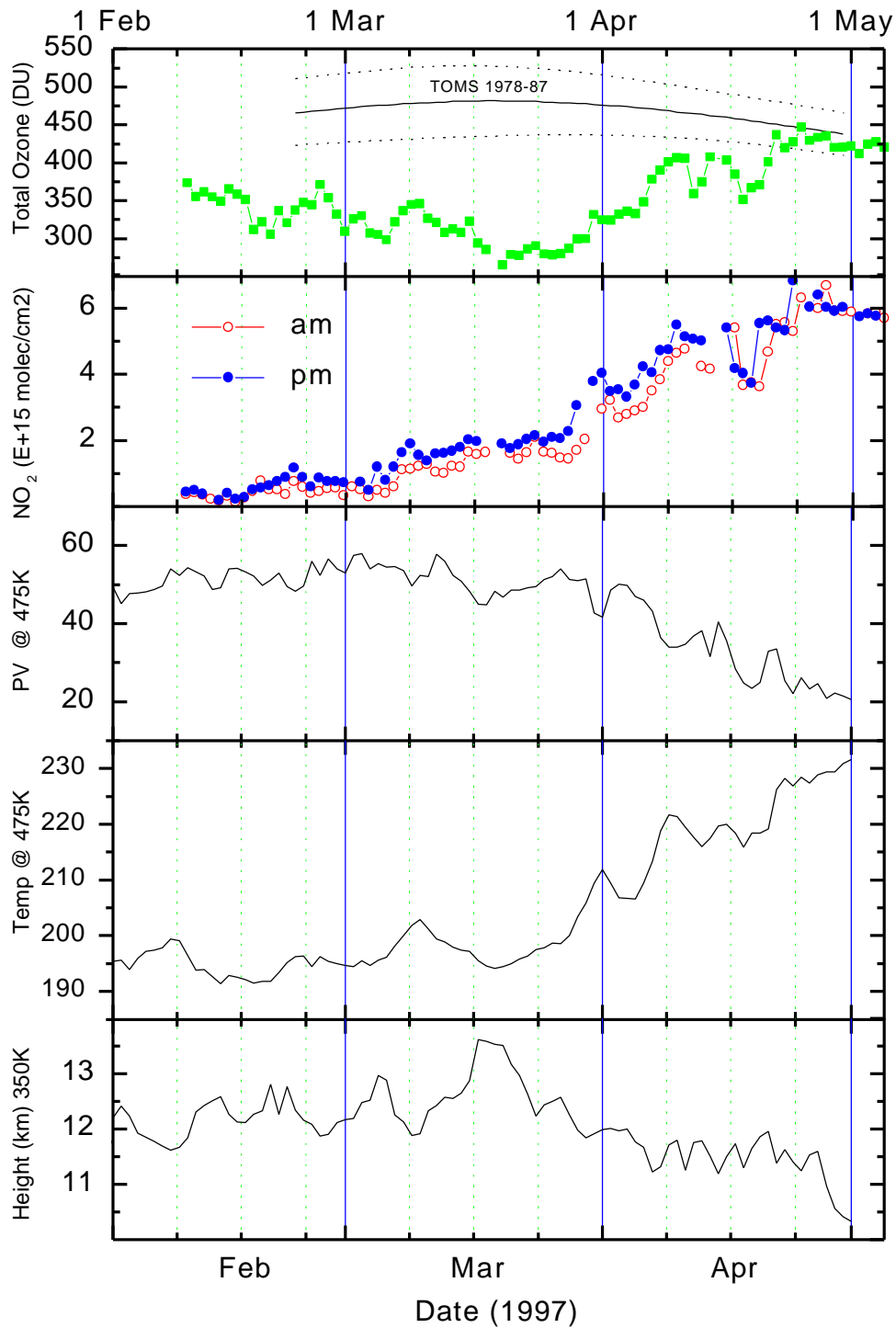


Figure 8 Vertical columns of ozone and NO₂ spring 1997 at Thule, together with ECWMF potential vorticity at 475 K, the temperature of the 50 hPa level and the height of the 250 hPa pressure level. The solid line and the dashed lines on the top graph indicate the average and standard deviation of Nimbus TOMS v.7 in the period 1979-88.

The SAOZ instrument in Thule has now been operating for 8 years. The observations have shown a marked decrease in the average vertical column ozone (total ozone) for March and April as indicated in Figure 9. An almost dramatic decrease in the average March total ozone is seen to occur after about 1990, with the lowest value ever recorded in 1997. A similar decrease is observed for the total ozone averaged over the

last two weeks of February. However, compared to a cold stratosphere in spring 1997, with substantial ozone depletion, the stratosphere was relatively warm in spring 1998, with only little ozone depletion, and for both March and April the figure clearly shows the influence of stratospheric temperature on depletion of the total column ozone. Whereas the decrease in March seems to occur after about 1990 the decrease in April seems to be more even over time. The very low ozone in March in 1993, 1995, 1996 and 1997, were accompanied by observations of very low NO₂ columns. Whereas the SAOZ observations in Thule show a marked ozone depletion in spring the average monthly total column ozone in autumn – August, September and October – shows no significant change over the past 8 years.

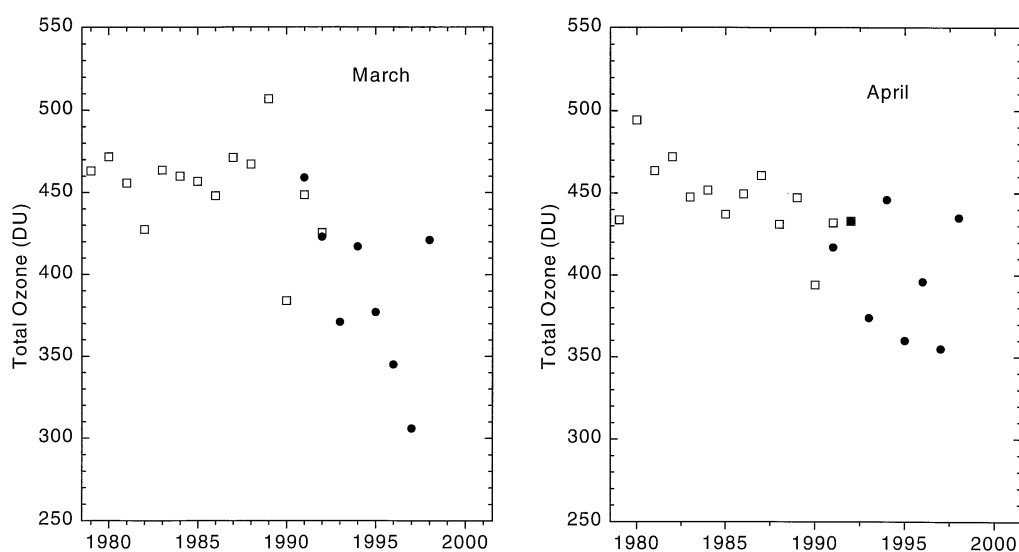


Figure 9 The monthly average total column ozone for March and April at Thule. Nimbus-7 TOMS ver. 7 monthly averages are shown in open squares and SAOZ monthly averages are shown in solid circles.

Microphysical modelling of polar stratospheric clouds.

Polar stratospheric clouds play an important role in priming the polar winter stratosphere for chemical ozone depletion. On the particle surfaces heterogeneous chemical reactions convert chlorine reservoir species into reactive ozone destruction forms. Secondly, the particles are composed of nitric acid and water that may be removed irreversibly from the stratosphere by particle sedimentation. This will imply low concentrations of reactive nitrogen which otherwise would reduce the adverse effects of active chlorine on ozone. The heterogeneous chemical reactions and the sedimentation properties depend strongly on the particle composition and physical phase. Presently, the freezing process and the mechanism to generate large solid PSC particles, responsible for denitrification in the Arctic stratosphere, are not well known.

At least two types of polar stratospheric clouds, forming above the ice frost point temperature, have been identified from observations and classified as type 1a and 1b PSC. Lidar depolarisation measurements have revealed that these clouds are

composed of solid and liquid phase particles respectively, and many observations and theoretical investigations point to the fact that type 1b PSC are composed of liquid supercooled ternary solutions (STS; $\text{HNO}_3/\text{H}_2\text{SO}_4/\text{H}_2\text{O}$)⁵. However, for type 1a PSCs the chemical composition and the conditions under which these particles form are still very uncertain. The particles are composed of nitric acid and water, and the most stable composition under stratospheric conditions would be nitric acid trihydrate (NAT)⁶. However the particles could initially form in a metastable phase, e.g. nitric acid dihydrate (NAD)⁷ or a dilute solid solution⁸. Type 2 PSC particles form below the ice frost point and are composed of water ice crystals. Both the chemical composition and physical phase of PSC particles influence the heterogeneous reactions, activating reservoir halogen compounds in the stratosphere, and details of the nature of the particles are required for a better modelling of atmospheric chemistry affecting the ozone layer.

Laboratory experiments have revealed⁹ that STS is unlikely to freeze homogeneously, unless the sulphuric acid weight fractions are very low, i.e. at temperatures several degrees below the ice frost point where the composition approaches binary nitric acid solutions. Synoptic temperatures in the Arctic may only very occasionally drop to such low values. However, it has been speculated that fast cooling events in mesoscale temperature fluctuations, e.g. in mountain leewaves, could induce a sufficient cooling to impose homogeneous freezing of type 1b PSC particles¹⁰. Furthermore, in fast cooling events the STS particles are brought strongly out of equilibrium due to slow diffusion of HNO_3 in the gas phase, causing a size dependent compositions of the type 1b PSC particles. In this case only the smallest particles obtain a nearly binary $\text{HNO}_3/\text{H}_2\text{O}$ composition which would favour the homogeneous freezing¹¹. In order to simulate these effects, a non-equilibrium microphysical model of STS particles is required together with a model to represent the homogeneous freezing process.

In Figure 10 is shown an example of a 6.5 hour PSC simulation with the new DMI model in a leewave situation (actually the same case as in Carslaw et al., 1998, their Figure 2, where the temperature history has been derived from airborne lidar observations at Kiruna). In these simulations it has been assumed that freezing takes place at 4.1 K below the ice frost point, and that solid ice particles melts into STS particles above T_{ice}). The model takes as input the ambient air state variables: temperature, pressure, partial pressure of water vapor, and partial pressure of nitric acid vapor. The partial pressures are changed according to the evaporation / condensation taking place. The model calculates the time dependent radius and physical phase of each particle type, holding the number of particles per kg. air in each radius class fixed (Lagrangian approach in radius space). The mass of condensed H_2SO_4 , HNO_3 , and H_2O per particle (chemical composition) is calculated in each radius class due to condensation/evaporation, assuming a constant H_2SO_4 content.

⁵ Tabazadeh, A. et al., *Geophys. Res. Lett.* 21, 1619-1622, 1994.; Carslaw, K.S. et al., *Geophys. Res. Lett.*, 21, 2479-2482, 1994

⁶ Hanson, D., and K. Mauersberger, *Geophys. Res. Lett.* 15, 855-858, 1988.

⁷ Worsnop, D.R., et al., *Science* 259, 71-74, 1993.

⁸ Tabazadeh, A. and O.B. Toon, *J. Geophys. Res.* 101, 9071-9078, 1996.

⁹ e.g. Koop et al., *J. Phys. Chem.* 101A, 1117-1133, 1997

¹⁰ e.g. Carslaw et al., *J. Geophys. Res.* 103, 5785-5796, 1998

¹¹ e.g. Meilinger et al., *Geophys. Res. Lett.* 22, 3031-3034, 1995

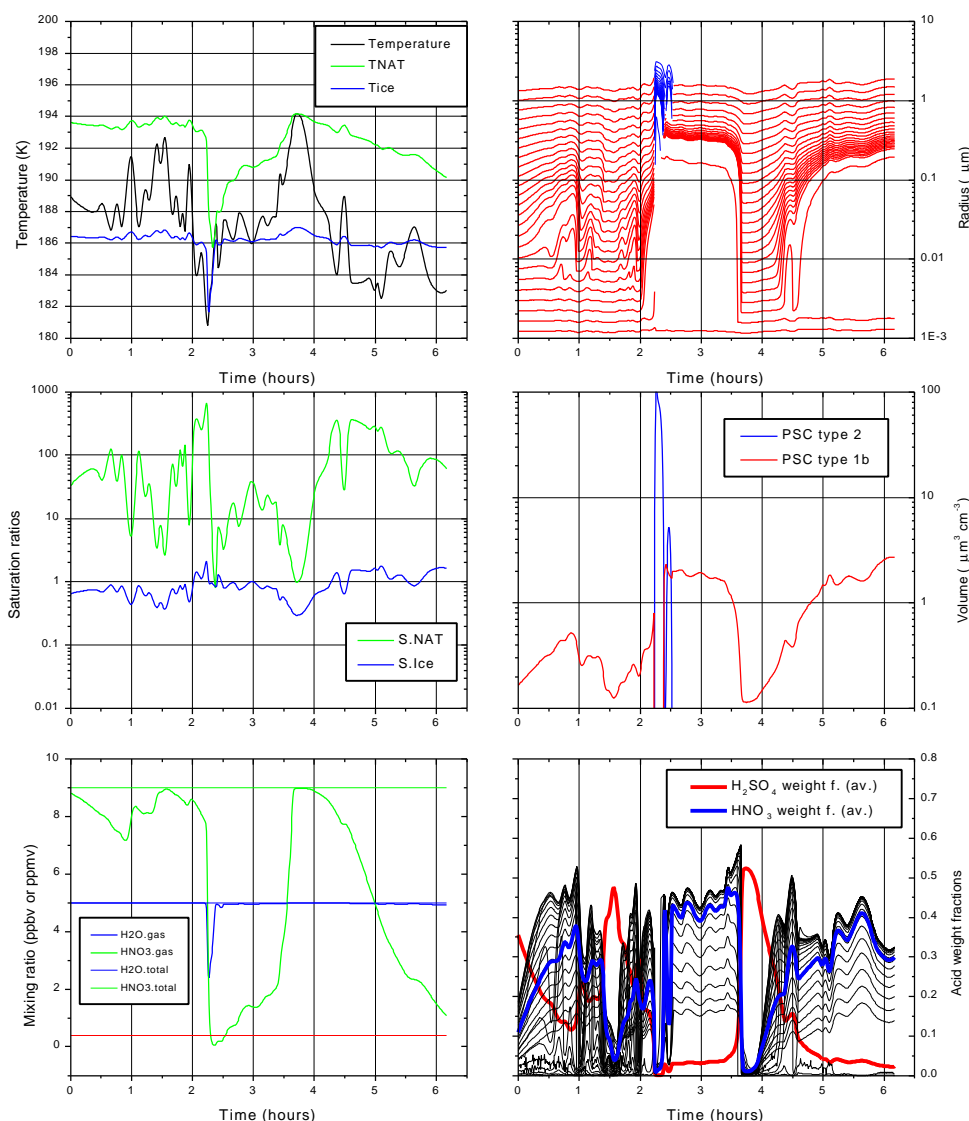


Figure 10 shows various PSC model-calculated variables in 6 panels. The **upper left panel** shows the temperature (black), the nitric acid trihydrate (NAT) condensation temperature (green), and ice frost point temperature (blue). The condensation temperatures are calculated corresponding to the actual gas phase concentrations. The **middle left panel** shows the saturation ratios over NAT (green) and ice (blue), and the **lower left panel** shows the gas phase mixing ratios of HNO_3 (green) and H_2O (blue). The **upper right panel** shows the radius of particles in each size class, red curves for liquid and blue curves for solid particles. The **middle right panel** shows the volumes of different types of particles: red: STS type 1b PSC (sulfate aerosols); blue: solid type 2 PSC. The **lower right panel** shows the nitric acid weight fractions in the different size classes (black), the volume averaged nitric acid weight fraction (blue), and volume averaged sulfuric acid weight fraction in all particles. This simulation example illustrates the effects of the rapid temperature fluctuations. Particles with small radii quickly adjust to the changing temperatures and obtain very high HNO_3 weight fractions approaching 50%. Upon freezing more than half of the available H_2O vapor condenses forming relative large ice particles with radii larger than $1 \mu\text{m}$.

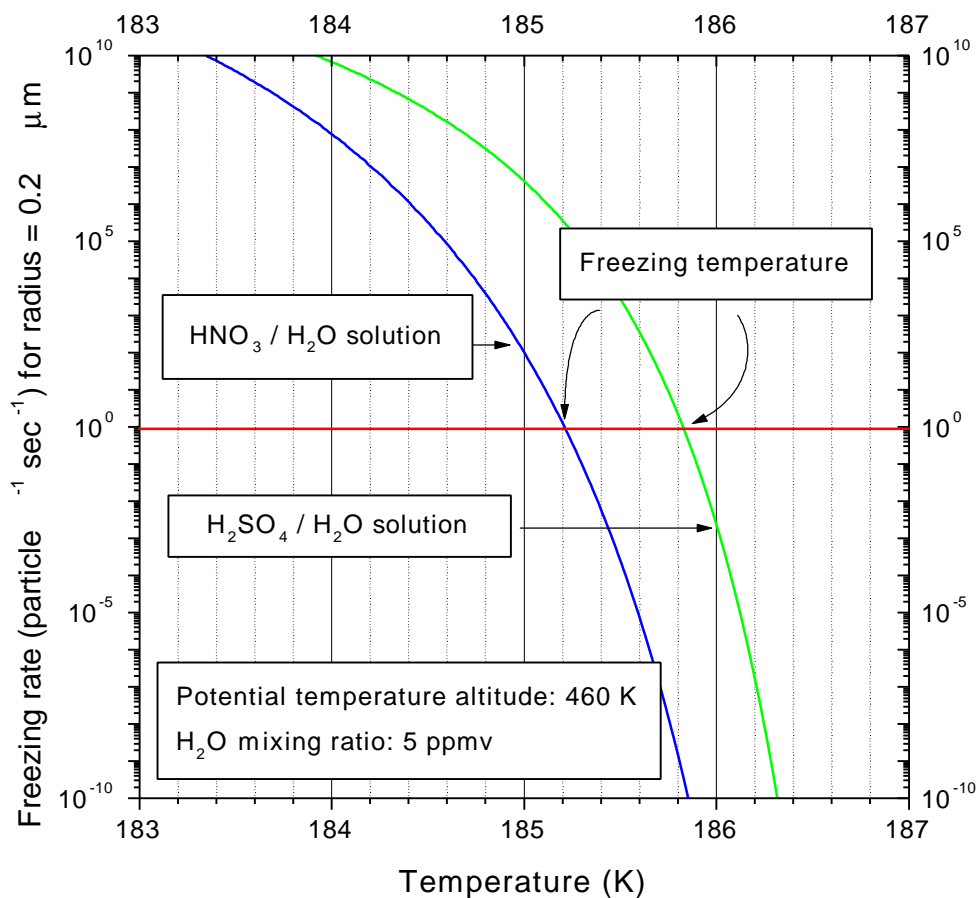


Figure 11 Calculated freezing rates for binary $\text{HNO}_3/\text{H}_2\text{O}$ and $\text{H}_2\text{SO}_4/\text{H}_2\text{O}$ solutions droplets of radius $0.2 \mu\text{m}$ at 460 K potential temperature altitude, assuming 5 ppmv H_2O vapour.

A microphysical module for homogeneous freezing of supercooled PSC type 1b droplets has been developed at the DMI to be used for investigations of freezing process to generate type 1a PSCs. This model is based on the method suggested by Tabazadeh et al. (*Geophys. Res. Lett.* 24, 2007, 1997), utilising estimates of various thermodynamical properties from laboratory freezing experiments of sulphate aerosols (Bertram et al., *J. Phys. Chem.* 100, 2376, 1996). Mainly three factors control the freezing temperatures: the H_2O partial pressure and the assumed values of the diffusion activation energy and the surface tension between the liquid and the ice germs. Figure 11 shows the calculated freezing rates (and freezing temperatures) for binary $\text{HNO}_3/\text{H}_2\text{O}$ and $\text{H}_2\text{SO}_4/\text{H}_2\text{O}$ solution droplets of radius $0.2 \mu\text{m}$ as functions of the temperature, assuming a water vapour concentration of 5 ppmv at 460 K potential temperature. The calculated freezing temperatures are well below the ice frost point temperature (187 K at these conditions).

The new microphysical PSC model at DMI applies “Lagrangian” particle growth in radius space; i.e. the model calculates the time dependent radius of individual particles in a number of size classes, each size class having a fixed number of particles per kg of air. The previous version of the DMI microphysical PSC model applies “Eulerian” particle

growth where particles are shifted between fixed size bins. As shown above, the Lagrangian approach allows for the non-equilibrium simulation of particle growth, and the calculation of the particle size distribution is exactly reversible in repeated condensation/evaporation cycles. On the other hand, the Eulerian model version, which only allows for equilibrium simulation of type 1b PSC particles, is more suited for long term simulations and studies of sedimentation processes. Both model versions apply the same basic modules for microphysical and thermodynamical calculations. The freezing module can be used in both model versions.

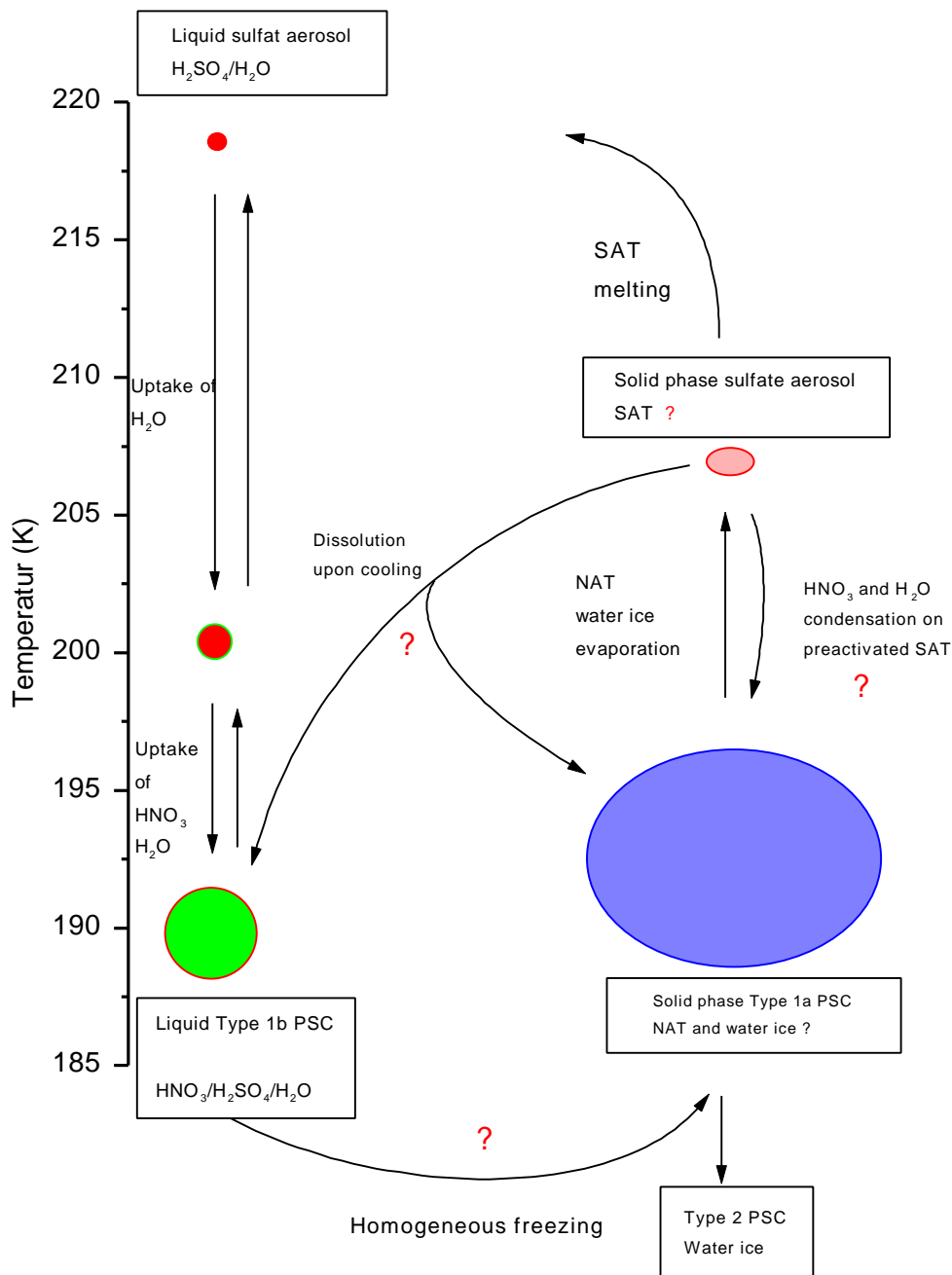


Figure 12 Schematic illustration of possible pathways for phase changes between liquid and solid phase PSC particles.

One of the main problems for simulation of PSCs is how to represent phase changes, i.e. freezing and melting. In Figure 12 is indicated how the DMI microphysical model currently assumes these processes to occur and the different possible pathways that the model allows to be simulate. The left-hand side of the figure illustrates the growth/shrink of liquid particles, forming type1b PSC particles (STS) at the lowest temperatures. Below the ice frost point, homogeneous freezing (simulated with the above-mentioned module) may generate the formation of solid particles. Once the solid particles are formed these particles are grouped into three categories in the model, depending on the chemical composition. The available water in each solid particle is assumed to be bound by 4 H₂O molecules to each one H₂SO₄ molecule, forming sulphuric acid tetrahydrate (SAT), and by 3 H₂O molecules to each one HNO₃ molecule, forming nitric acid trihydrate (NAT). Any H₂O molecules left not bound in hydrates are assumed to form water ice (excess ice). Particles with excess ice are classified as type 2 PSCs. The solid particles initially form in this category. Particles with no excess ice but holding HNO₃ (NAT) are classified as type 1a PSCs. Particles with no excess water and no HNO₃ (NAT) are classified as solid stratospheric aerosols (SAT particles). The solid particles are represented on the right-hand side of Figure 12. Upon heating the type 2 PSC particles first transform into type 1a PSC, evaporating the excess water, and then into SAT particles, evaporating the nitric acid. When a SAT particle is released, several pathways could be applied in a subsequent cooling. Either NAT could condense on this preactivated (Zhang et al., *Geophys. Res. Lett.* 23, 1669-1672, 1996) SAT particle, forming a type 1a PSC particle again. Alternatively, the SAT particles could dissolve upon cooling, forming a liquid type 1b PSC particle (Koop and Carslaw, *Science* 272, 1638-1641, 1996) or forming a NAT particle again (Iraci et al., *J. Geophys Res.*, 103,8491-8498, 1998). Finally the SAT particle would melt if heated. No matter which pathway may be the more realistic, the important temperature hysteresis with solid particles forming below the ice frost point and existing up to T_{NAT} or even higher, is represented by the model.

Balloonborne backscatter soundings of polar stratospheric clouds.

PSCs have been observed by balloonborne backscatter sondes from Thule and Sondre Stromfjord. Figure 13 presents 7 vertical profiles of the aerosol backscatter ratio at 940 nm together with the measured temperatures. Four balloonborne backscatter soundings have been performed from Thule in the spring 1997. Vertical profiles of the aerosol backscatter ratio and temperature are shown in the Figure 14. PSC were not forming over Thule in winter/spring early 1998 and for that reason soundings were not performed. Final data have been stored at the NILU data base.

The balloonborne backscatter sonde was developed by the University of Wyoming for measurements of stratospheric aerosol and cloud particles. The instrument is equipped with a flash lamp, emitting strong horizontally directed beams approximately every 7 seconds during the balloon ascent and descent.

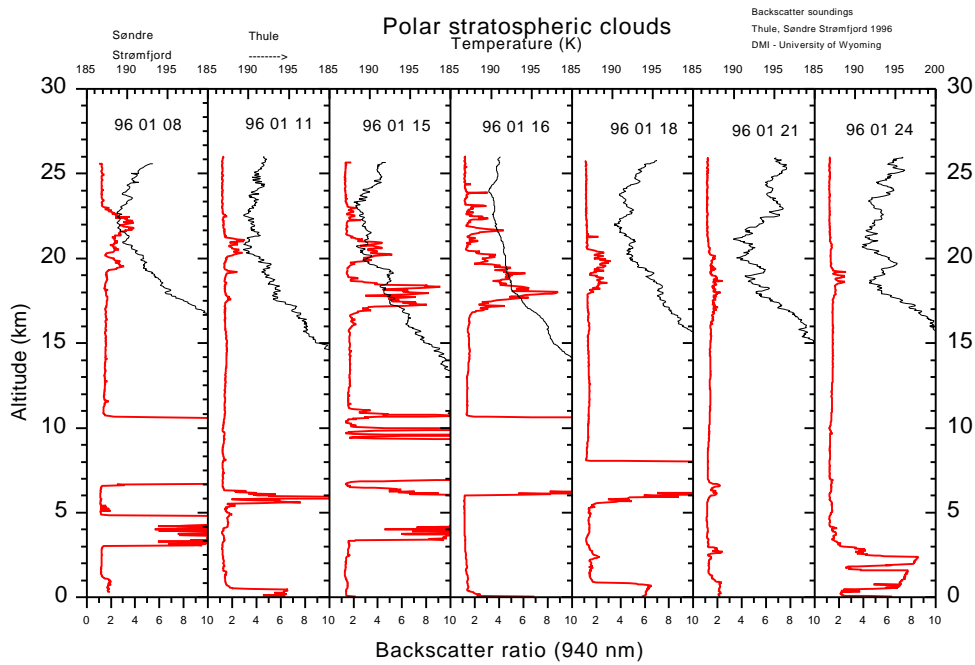


Figure 13 Vertical profiles of backscatter ratio (red curves) and temperature (black) measured by balloonborne backscatter sondes in winter 1995/96. The measurements show the presence of polar stratospheric clouds (PSC) at very low temperatures in the altitude range 17-23 km. The clouds are observed at the same altitude ranges where the severe ozone depletion took place.

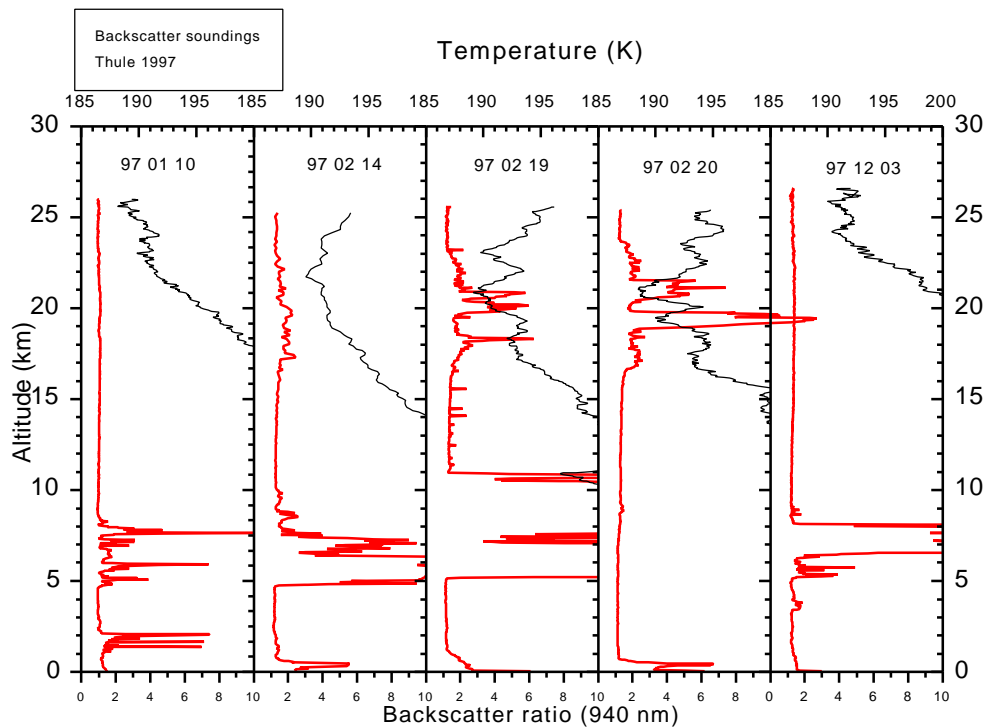


Figure 14 Backscatter soundings at Thule in from 1997.

The backscattered light from the particles, within a range of a few meters from the sonde, is measured by photodetectors with narrow band filters in two wavelengths around 940 and 480 nm. A colour index is defined as the ratio between the aerosol backscatter at 940 and 480 nm. The ambient air pressure and temperature, together with ozone partial pressure, are measured simultaneously with the aerosol backscatter signal.

The PSC observations have been supplemented by previous measurements from Ny Ålesund, Alert, Heiss Island, Scoresbysund, Sodankylä, and Sondre Stromfjord during winters (January) 1989, 1990, 1991, 1995, and 1996 for a study of the nature of the particles [Larsen *et al.*, 1996, 1997].

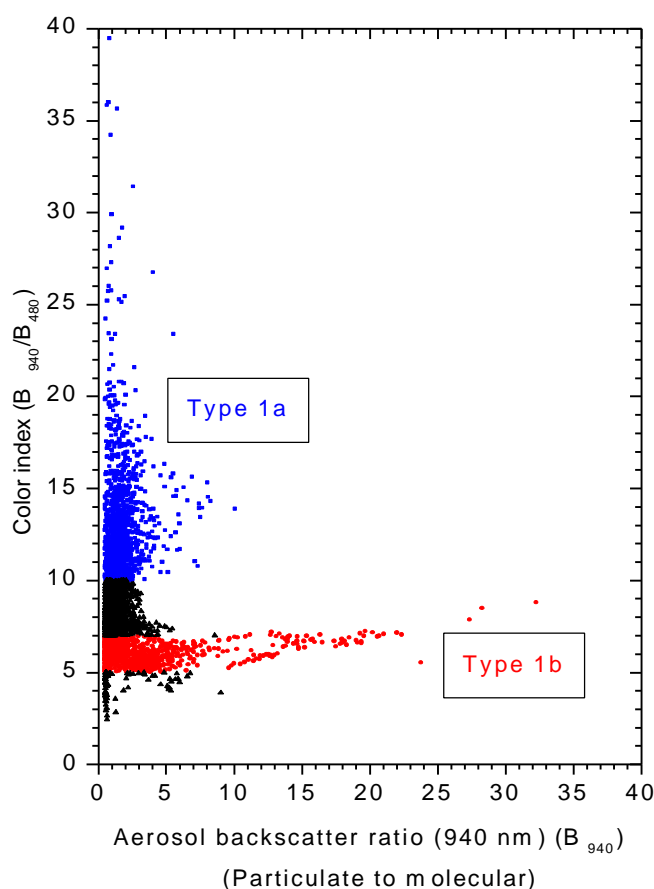


Figure 15 Balloonborne backscatter measurements indicate the existence of two categories of Type 1 PSCs (also a common feature in lidar observations): Type 1a PSCs show moderate aerosol backscatter with large color indices > 10 (blue); Type 1b PSCs show a large variability in aerosol backscatter with color indices around $\sim 5 - 7$ (red symbols).

By plotting the measured colour indices of the PSC particles (ratio between the backscatter ratio at 940 and 480 nm) against the backscatter ratio at 940 nm the observations can be categorised into two main groups: Type 1a and Type 1b PSC particles, cf. Figure 15. Type 1a PSC particles show moderate aerosol backscatter with large colour indices > 10 (blue squares) while Type 1b PSC particles show a large variability in aerosol backscatter with colour indices around $\sim 5 - 7$ (red circles). Similar groupings of PSC particles from lidar observations have been known for many years, and

originally gave rise to the distinction between the two subtypes of type 1 PSCs¹². With the same colour coding as in Figure 15, the measured aerosol backscatter ratios and colour indices from all observations are plotted against the difference between the measured air temperature and the nitric acid trihydrate (NAT) condensation temperature in Figure 16. From these plots it appears that type 1b PSCs (red symbols), at high temperatures, possess low aerosol backscatter ratios which, at roughly 4 K below T_{NAT} , increase sharply (upper panel). On the other hand, type 1a PSCs (blue symbols) are observed predominantly at temperatures just below the NAT condensation temperature (lower panel).

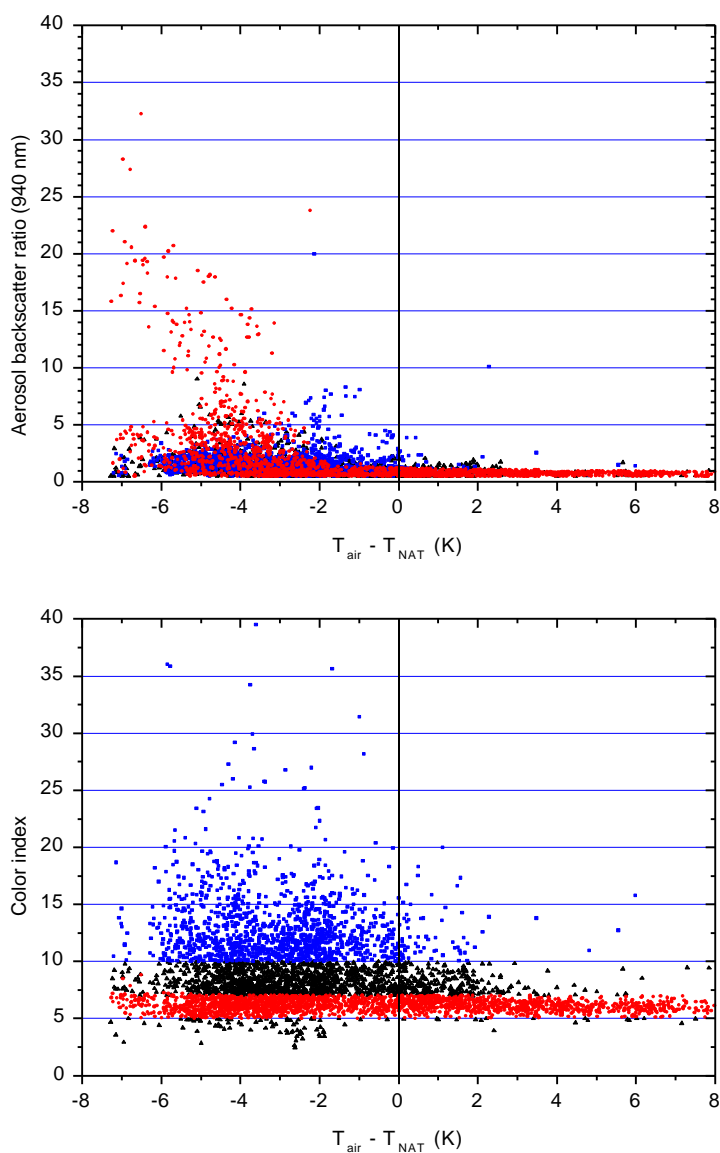


Figure 16 Aerosol backscatter ratio and color index of the same observations and color coding as in Figure 15, plotted against the difference between the measured air temperature and the NAT condensation temperature.

¹² Browell et al., *Geophys. Res. Lett.* **17**, 385-388, 1990; Toon, O.B., et al., *Geophys. Res. Lett.* **17**, 393-396, 1990

Further analysis of the observations reveal that Type 1b PSC show the characteristics as expected from liquid ternary solution ($\text{HNO}_3/\text{H}_2\text{SO}_4/\text{H}_2\text{O}$) particles, consistent with model simulations. Type 1a PSC show some characteristics, consistent with solid nitric acid trihydrate (NAT) composition.

The trajectory calculations have been used to investigate the influence of synoptic temperature histories on the physical properties of PSC particles. Air parcel trajectories have been calculated for all observations, providing the temperature histories of the observed particles. A number of cases have been identified, where the particles have experienced temperatures close to or above the sulphuric acid tetrahydrate (SAT) melting temperatures within 20 days prior to observation. This assures, with some confidence, knowledge of the physical phase (liquid) of the particles at some time prior to observation. The subsequent temperature histories, until the time of observation, show pronounced differences for Type 1a and Type 1b PSC particles, indicating the qualitative temperature behaviour in the freezing process to generate solid Type 1a PSCs.

It appears from the observations that liquid type 1b PSC particles can be cooled to very low temperatures, approaching the ice frost point, without causing them to freeze. In a subsequent monotonic heating the particles will survive in the liquid state. Most of the liquid type 1b particles are observed in the process of an ongoing, relatively fast, and continuous cooling from temperatures clearly above the NAT condensation temperature. The particles are mostly seen at the edge of a cloud shortly after they enter the cold area. On the other hand, it appears that a relatively long period, with a duration of at least 1-2 days, at temperatures below T_{NAT} , and possibly also accompanied by slow, synoptic temperature fluctuations, provide the conditions which may lead to the production of solid type 1a PSCs. Solid PSC particles are therefore expected to be observed in aged clouds. These findings are illustrated in Figure 17, showing a histogram of the time spent at temperatures below T_{NAT} before the PSC particles were observed.

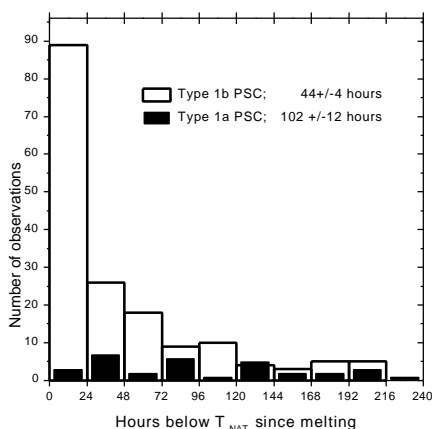


Figure 17 Histogram of time spent below T_{NAT} between SAT melting and observation. The Figure shows the histogram for type 1a and 1b PSC observations, categorized according to the average color index within the 5 K potential temperature window around the corresponding trajectory altitude. 169 averaged observations (trajectories) are used for the type 1b, and 33 are used for the type 1a PSC distributions.

Backscatter sonde measurements have been used for investigation of freezing conditions of PSC particles in comparison with model calculations. The 20-days backward isentropic trajectories are calculated to identify the minimum temperatures, experienced by the particles prior to observation. In some cases, the temperatures have been above the SAT melting within the last 20 days prior to observation. In those cases, freezing presumably took place after this last melting event. Figure 18 shows the synoptic minimum temperatures experienced by liquid and solid PSC particles within 20 days prior to observation as derived from the air parcel temperature histories. The solid curve shows the calculated homogeneous freezing temperatures of $\text{HNO}_3/\text{H}_2\text{O}$ droplets, assuming the indicated H_2O concentration profile, and the dotted curves give the uncertainty in the freezing temperatures, assuming an error of 1 ppmv H_2O . In most cases, the synoptic minimum temperatures are above the homogeneous freezing temperatures and most of the minimum temperatures are also above the ice frost point (dashed curve). The expected freezing temperatures are very low, and the large uncertainty in the assumed values of the diffusion activation energy and the surface tension does not seem to explain the observations. Thus, no clear evidences have emerged from this study, based on synoptic temperature histories, to suggest that homogeneous freezing of $\text{HNO}_3/\text{H}_2\text{O}$ solution is responsible for the formation of the observed type 1a PSCs. Efforts are in progress to investigate possible effects from mesoscale temperature fluctuations on the freezing of the observed PSC particles.

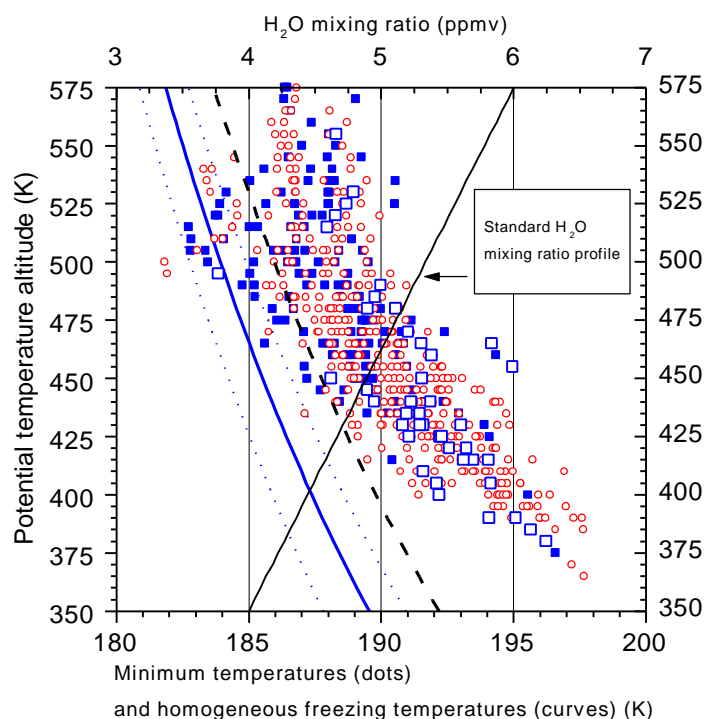


Figure 18 Synoptic minimum temperatures experienced by solid type 1a (blue) and liquid type 1b (red) PSCs within 20 days prior to observation, and compared to the expected homogeneous freezing temperatures of $\text{HNO}_3/\text{H}_2\text{O}$ droplets (solid curve) and the ice frost point temperatures (dashed curve). Open square symbols indicate observations where temperatures have been above the SAT melting temperature prior to observation.

UV-B radiation measurements

Measurements of UV radiation at Thule began in late 1992 with a Robertson-Berger broadband instrument from the National Radiological Protection Board in the U.K. In late 1994 a spectroradiometer was installed but relocated to another building in spring 1995. The spectroradiometer has been in regular operation since April 1995 from the same location as the SAOZ instrument and the broad-band UV instrument.

The UV radiation measurements for 1996 clearly revealed increased short wavelength radiation when the vortex was present over Thule and the ozone was very low (Figure 7). The instrument has been working in a mode where a full spectrum (290 - 410 nm) has been recorded every 10 minutes. Unfortunately the spectroradiometer suffered from a temperature-controller failure in the period 16 May - 5. June and from a filter-wheel malfunction in the period 13. July - 25. July 1996. For these periods we only have imperfect daily coverage. Figure 19. shows the erythemally-weighted (CIE) daily radiant exposure (dose).

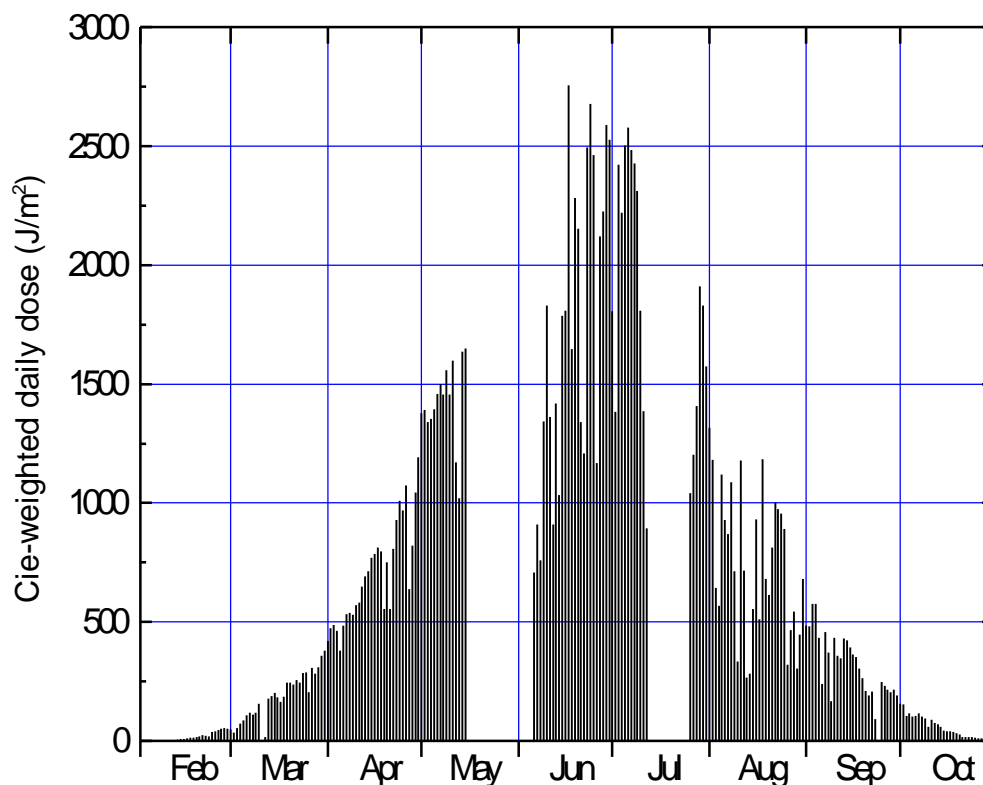


Figure 19 DMI spectroradiometer measurements of ultraviolet radiation, Thule 1996. There is only partly daily coverage for the periods 16 May - 05 June and 13 July - 25 July as explained in the text.

The substantial ozone layer depletion over Northern Greenland in March 1997 clearly showed up in the UV radiation measurements at Thule. Figure 20 shows the ratio of the measured global spectral irradiances at 305 and 320 nm for a solar zenith angle of 85 degrees (± 0.25) together with the total ozone as measured with the co-located SAOZ spectrometer. The use of the UV ratio filters out most of the influence of clouds and the remaining lack of complete anticorrelation is mostly caused by scatter in the solar zenith angle. The average monthly UV-B exposure (dose) in March 1997 is the highest recorded since 1993, well anticorrelated with the lowest recorded monthly average ozone since the ozone measurements began in Thule.

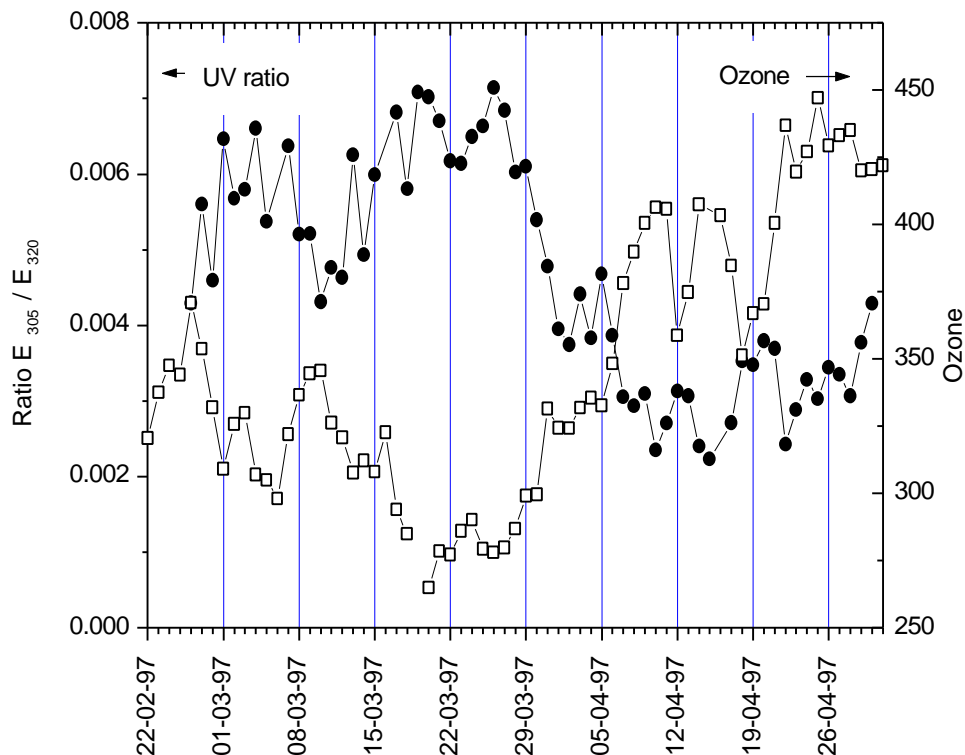


Figure 20 Ratio of measured spectral irradiances at 305 and 320 nm and the daily averaged total ozone at Thule for spring 1997.

The spectroradiometer has specification to meet the NDSC demands and the instrument data will be evaluated during 1999 in order to be NDSC qualified. Because of the longer series of measurements with the broad-band instrument data from this instrument is shown in Figure 21 for March and April. Because both total ozone and cloud cover has a pronounced effect on UV-B irradiance the monthly average total ozone and the monthly average cloud cover is also shown in the figure.

As an example one may consider for March the years 1996, 1997 and 1998 and notice the anticorrelation with ozone. However, the monthly average UV-B is about the same for 1996 and 1998 whereas the ozone in 1996 is lower than in 1998 indicating, that if the cloud cover was the same, the UV-B in 1996 should have been higher than in 1998. The reason that the 1996 and 1998 UV-B levels are about the same is that the cloud cover in 1996 was higher than in 1998 combined with lower ozone in 1996

compared to 1998. The same argument applies to the last 3 years for April. From the limited length of the time series it is difficult to ascribe an UV-B trend to the March and April average monthly UV-B irradiance.

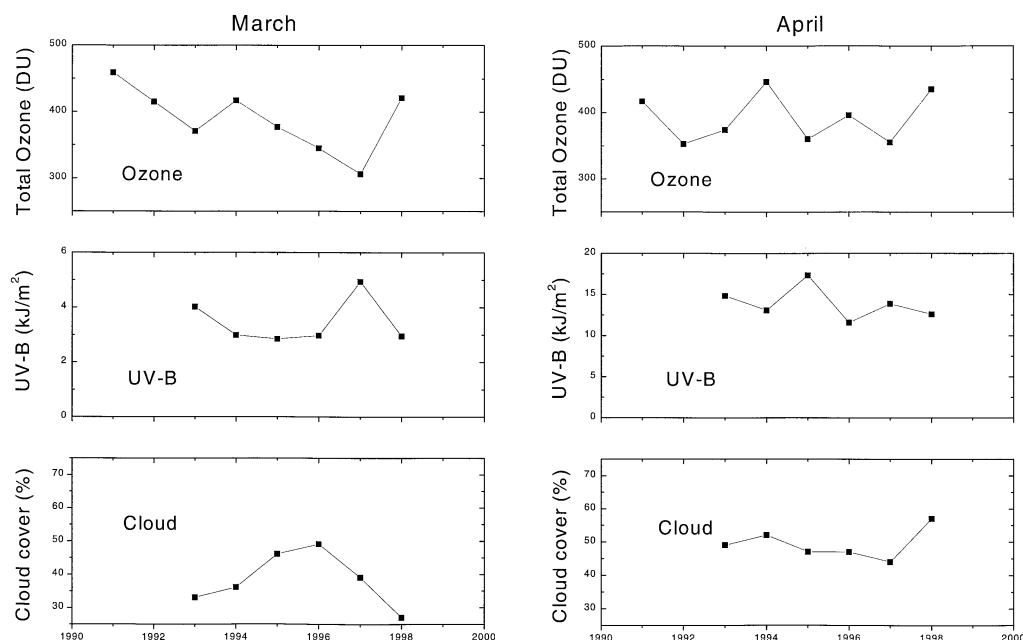


Figure 21 The monthly average total ozone, the total monthly CIE-weighted UV radiant exposure (dose) and the monthly average cloud cover for March and April at Thule.

Conclusions.

Stratospheric measurements and data analysis related to ozone depletion began at the DMI observatories at Thule, Sondre Stromfjord and Scoresbysund, Greenland, in the beginning of the 1990's. Some of the research activities were part of major European field campaigns THESEO (DMI scientific report 92-1), SESAME, and THESEO. Other activities were performed as part the predecessor projects to the ESMOS/Arctic II project, "Experimentation related to polar stratospheric clouds", "Investigations of ozone, aerosols, and clouds in the Arctic stratosphere" (DMI scientific report 95-3), and "European Stratospheric Monitoring Stations in the Arctic" (DMI scientific report 96-11).

Combined with long-term measurements from the other ESMOS stations, the data set constitutes an important documentation of the development of the North Polar ozone layer. The measurements have been obtained during an important period where concentrations of stratospheric concentrations of man-made halogen species are approaching their expected maximum concentrations, and a slow recovery of the ozone layer could be expected due to the restrictions on the usage of CFCs and Halons, as laid

out in the Montreal Protocol and its Amendments. The period of documentation is also important in the sense that signs begin to appear of decreasing temperatures in the polar stratosphere, possible due to a coupling to increased concentrations of greenhouse gases and the general depletion of the ozone layer¹³. Some of the Arctic winters in the 1990's (in particular 1995/1996 and 1996/1997) were extremely cold, leading to pronounced formation of polar stratospheric clouds and substantial ozone depletion, demonstrating the importance of the temperature for chemical ozone depletion. This report has presented ozone-, UVB-, and PSC measurements and theoretical analysis from these winters.

Scientific concern is arising that a general trend of decreasing temperatures in the Arctic stratosphere may lead to more regular and widespread ozone depletion, resembling conditions as over Antarctica. In order to investigate climatological aspects for ozone, long-term monitoring of the state of the ozone layer as performed at the ESMOS/NDSC stations is of mandatory importance.

¹³ Pawson et al., *Geophys. Res. Lett.* 25, 2157-2160, 1998; Ramaswamy, V et al., *Nature*, 382, 616-618, 1996.

Publications:

Knudsen, B. M., J. M. Rosen, N. T. Kjome, and A. T. Whitten, Comparison of analyzed stratospheric temperatures and calculated trajectories with long-duration balloon data, *J. Geophys. Res.*, 101, 19,137-19,145, 1996.

Knudsen, B. M., Accuracy of arctic temperature analyses and the implications for the prediction of polar stratospheric clouds, *Geophys. Res. Lett.*, 23, 3747-3750, 1996.

B. M. Knudsen, N. Larsen, I.S. Mikkelsen, J.-J. Morcrette, G.O. Braathen, E. Kyrö, H. Fast, H. Gernandt, H. Kanzawa, H. Nakane, V. Dorokhov, V. Yuskov, G. Hansen, M. Gil, and R.J. Shearman, Ozone depletion in and below the Arctic vortex for 1997, *Geophysical Research Letters*, 25, 627-630, 1998

N.Larsen, B. Knudsen, J.M. Rosen, N.T. Kjome, and E. Kyrö, Balloonborne backscatter observations of type 1 PSC formation: Inference about physical state from trajectory analysis, *Geophysical Research Letters* 23, 1091-1994, 1996.

N. Larsen, B.M. Knudsen, J.M. Rosen, N.T. Kjome, R. Neuber, and E. Kyrö: Temperature histories in liquid and solid polar stratospheric cloud formation, *Journal of Geophysical Research* , **102**, 23505-23517, 1997.

N. Larsen, and B. Knudsen, Microphysical simulations of freezing of polar stratospheric clouds, in N.R.P. Harris, I. Kilbane-Dawe, and G.T. Amanatidis (ed), *Polar stratospheric ozone 1997, Proceedings of the fourth European symposium, Schliersee, 22-26 September 1997, Air Pollution Research Report no. 66, European Commission, p. 143-146, 1998.*

E.R. Lutman, J.A. Pyle, M.P. Chipperfield, D.J. Lary, I. Kilbane-Dawe, J.W. Waters, and N.Larsen, Three Dimensional Studies of the 1991/92 Northern Hemisphere Winter Using Domain-Filling Trajectories with Chemistry, *J. Geophys. Res.*,**102**, 1479-1488, 1997.

J.M. Rosen, N.T. Kjome, N. Larsen, B.M. Knudsen, E. Kyrö, R. Kivi, J. Karhu, R. Neuber, and I. Beninga, Polar stratospheric threshold temperatures in the 1995-1996 arctic vortex, *Journal of Geophysical Research*, 102, 28195-28202, 1997.

Presentations:

Knudsen, B. M., J. M. Rosen, N. T. Kjome, and A. T. Whitten, Accuracy of ECMWF stratospheric temperature analyses and the implications for PSC formation in the Arctic, Quadr. Ozone. Symp., L'Aquila, September 1996

B. M. Knudsen, N. Larsen, I.S. Mikkelsen, J.-J. Morcrette, G.O. Braathen, E. Kyrö, H. Fast, H. Gernandt, H. Kanzawa, H. Nakane, V. Dorokhov, V. Yuskov, G. Hansen, M. Gil, and R.J. Shearman, Ozone depletion in and below the Arctic vortex for 1997, Fourth European Symposium on Polar Stratospheric Ozone Research, Schliersee, Germany, September 1997, (poster).

N. Larsen, B.M. Knudsen, T.S. Jørgensen, J.M. Rosen og N.T. Kjome, Observations of type 1 PSC formation: Inference about Solid Particle Formation, XVIII Quadrennial Ozone Symposium, L'Aquila, Italy, September 1996.

N. Larsen, B.M. Knudsen, J.M. Rosen og N.T. Kjome, Balloonborne observations of polar stratospheric clouds: Discussion on the solid particle formation, NOSA/NORSAC symposium, Helsingør, Denmark, 15-17 November 1996.

N. Larsen and B.M. Knudsen, Microphysical simulations of the freezing of polar stratospheric clouds, Fourth European Symposium on Polar Stratospheric Ozone Research, Schliersee, Germany, September 1997, (poster).

DANISH METEOROLOGICAL INSTITUTE

Scientific Reports

Scientific reports from the Danish Meteorological Institute cover a variety of geophysical fields, i.e. meteorology (including climatology), oceanography, subjects on air and sea pollution, geomagnetism, solar-terrestrial physics, and physics of the middle and upper atmosphere.

Reports in the series within the last five years:

No. 94-1

Bjørn M. Knudsen: Dynamical processes in the ozone layer

No. 94-2

J. K. Olesen and K. E. Jacobsen: On the atmospheric jet stream with clear air turbulences (CAT) and the possible relationship to other phenomena including HF radar echoes, electric fields and radio noise

No. 94-3

Ole Bøssing Christensen and Bent Hansen Sass: A description of the DMI evaporation forecast project

No. 94-4

I.S. Mikkelsen, B. Knudsen, E. Kyrö and M. Rummukainen: tropospheric ozone over Finland and Greenland, 1988-94

No. 94-5

Jens Hesselbjerg Christensen, Eigil Kaas, Leif Laursen: The contribution of the Danish Meteorological Institute (DMI) to the EPOCH project "The climate of the 21st century" No. EPOC-003-C (MB)

No. 95-1

Peter Stauning and T.J. Rosenberg:
High-Latitude, day-time absorption spike events
1. morphology and occurrence statistics
Not published

No. 95-2

Niels Larsen: Modelling of changes in stratospheric ozone and other trace gases due to the emission changes : CEC Environment Program Contract No. EV5V-CT92-0079. Contribution to the final report

No. 95-3

Niels Larsen, Bjørn Knudsen, Paul Eriksen, Ib Steen Mikkelsen, Signe Bech Andersen and Torben Stockflet Jørgensen: Investigations of ozone, aerosols, and clouds in the arctic stratosphere : CEC Environment Program Contract

No. EV5V-CT92-0074. Contribution to the final report

No. 95-4

Per Høeg and Stig Syndergaard: Study of the derivation of atmospheric properties using radio-occultation technique

No. 95-5

Xiao-Ding Yu, **Xiang-Yu Huang** and **Leif Laursen** and Erik Rasmussen: Application of the HIRLAM system in China: heavy rain forecast experiments in Yangtze River Region

No. 95-6

Bent Hansen Sass: A numerical forecasting system for the prediction of slippery roads

No. 95-7

Per Høeg: Proceeding of URSI International Conference, Working Group AFG1 Copenhagen, June 1995. Atmospheric research and applications using observations based on the GPS/GLONASS System

No. 95-8

Julie D. Pietrzak: A comparison of advection schemes for ocean modelling

No. 96-1

Poul Frich (co-ordinator), H. Alexandersson, J. Ashcroft, B. Dahlström, G.R. Demarée, A. Drebs, A.F.V. van Engelen, E.J. Førland, I. Hanssen-Bauer, R. Heino, T. Jónsson, K. Jonasson, L. Keegan, P.Ø. Nordli, **T. Schmith, P. Steffensen, H. Tuomenvirta, O.E. Tveito:** North Atlantic Climatological Dataset (NACD Version 1) - Final report

No. 96-2

Georg Kjærgaard Andreassen: Daily response of high-latitude current systems to solar wind variations: application of robust multiple regression. Methods on Godhavn magnetometer data

No. 96-3

Jacob Woge Nielsen, Karsten Bolding Kristensen, Lonny Hansen: Extreme sea level highs: a statistical tide gauge data study

No. 96-4

Jens Hesselbjerg Christensen, Ole Bøssing Christensen, Philippe Lopez, Erik van Meijgaard, Michael Botzet: The HIRLAM4 Regional Atmospheric Climate Model

No. 96-5

Xiang-Yu Huang: Horizontal diffusion and filtering in a mesoscale numerical weather prediction model

No. 96-6

Henrik Svensmark and Eigil Friis-Christensen: Variation of cosmic ray flux and global cloud coverage - a missing link in solar-climate relationships

No. 96-7

Jens Havskov Sørensen and Christian Ødum Jensen: A computer system for the management of epidemiological data and prediction of risk and economic consequences during outbreaks of foot-and-mouth disease. CEC AIR Programme. Contract No. AIR3 - CT92-0652

No. 96-8

Jens Havskov Sørensen: Quasi-automatic of input for LINCOM and RIMPUFF, and output conversion. CEC AIR Programme. Contract No. AIR3 - CT92-0652

No. 96-9

Rashpal S. Gill and Hans H. Valeur: Evaluation of the radarsat imagery for the operational mapping of sea ice around Greenland

No. 96-10

Jens Hesselbjerg Christensen, Bennert Machenhauer, Richard G. Jones, Christoph Schär, Paolo Michele Ruti, Manuel Castro and Guido Visconti: Validation of present-day regional climate simulations over Europe: LAM simulations with observed boundary conditions

No. 96-11

Niels Larsen, Bjørn Knudsen, Paul Eriksen, Ib Steen Mikkelsen, Signe Bech Andersen and Torben Stockflet Jørgensen: European Stratospheric Monitoring Stations in the Arctic: An European contribution to the Network for Detection of Stratospheric Change (NDSC): CEC

Environment Programme Contract EV5V-CT93-0333: DMI contribution to the final report

No. 96-12

Niels Larsen: Effects of heterogeneous chemistry on the composition of the stratosphere: CEC Environment Programme Contract EV5V-CT93-0349: DMI contribution to the final report

No. 97-1

E. Friis Christensen og C. Skøtt: Contributions from the International Science Team. The Ørsted Mission - a pre-launch compendium

No. 97-2

Alix Rasmussen, Sissi Kiiilsholm, Jens Havskov Sørensen, Ib Steen Mikkelsen: Analysis of tropospheric ozone measurements in Greenland: Contract No. EV5V-CT93-0318 (DG 12 DTEE): DMI's contribution to CEC Final Report Arctic Tropospheric Ozone Chemistry ARCTOC

No. 97-3

Peter Thejll: A search for effects of external events on terrestrial atmospheric pressure: cosmic rays

No. 97-4

Peter Thejll: A search for effects of external events on terrestrial atmospheric pressure: sector boundary crossings

No. 97-5

Knud Lassen: Twentieth century retreat of sea-ice in the Greenland Sea

No. 98-1

Niels Woetman Nielsen, Bjarne Amstrup, Jess U. Jørgensen: HIRLAM 2.5 parallel tests at DMI: sensitivity to type of schemes for turbulence, moist processes and advection

No. 98-2

Per Høeg, Georg Bergeton Larsen, Hans-Henrik Benzon, Stig Syndergaard, Mette Dahl Mortensen: The GPSOS project
Algorithm functional design and analysis of ionosphere, stratosphere and troposphere observations

No. 98-3

Mette Dahl Mortensen, Per Høeg: Satellite atmosphere profiling retrieval in a nonlinear troposphere
Previously entitled: Limitations induced by Multipath

No. 98-4

Mette Dahl Mortensen, Per Høeg:
Resolution properties in atmospheric profiling with GPS

No. 98-5

R.S. Gill and M. K. Rosengren
Evaluation of the Radarsat imagery for the operational mapping of sea ice around Greenland in 1997

No. 98-6

R.S. Gill, H.H. Valeur, P. Nielsen and K.Q. Hansen: Using ERS SAR images in the operational mapping of sea ice in the Greenland waters: final report for ESA-ESRIN's: pilot projekt no. PP2.PP2.DK2 and 2nd announcement of opportunity for the exploitation of ERS data projekt No. AO2..DK 102

No. 98-7

Per Høeg et al.: GPS Atmosphere profiling methods and error assessments

No. 98-8

H. Svensmark, N. Woetmann Nielsen and A.M. Sempreviva: Large scale soft and hard turbulent states of the atmosphere

No. 98-9

Philippe Lopez, Eigil Kaas and Annette Guldborg: The full particle-in-cell advection scheme in spherical geometry

No. 98-10

H. Svensmark: Influence of cosmic rays on earth's climate

No. 98-11

Peter Thejll and Henrik Svensmark: Notes on the method of normalized multivariate regression

No. 98-12

K. Lassen: Extent of sea ice in the Greenland Sea 1877-1997: an extension of DMI Scientific Report 97-5

No. 98-13

Niels Larsen, Alberto Adriani and Guido DiDonfrancesco: Microphysical analysis of polar stratospheric clouds observed by lidar at McMurdo, Antarctica

No.98-14

Mette Dahl Mortensen: The back-propagation method for inversion of radio occultation data

No. 98-15

Xiang-Yu Huang: Variational analysis using spatial filters

No. 99-1

Henrik Feddersen: Project on prediction of climate variations on seasonal to interannual timescales (PROVOST) EU contract ENV4-CT95-0109: DMI contribution to the final report: Statistical analysis and post-processing of uncoupled PROVOST simulations

No. 99-2

Wilhelm May: A time-slice experiment with the ECHAM4 A-GCM at high resolution: the experimental design and the assessment of climate as compared to a greenhouse gas experiment with ECHAM4/OPYC at low resolution
(In press)